January 1, 1993

Accounting for Saturation Effects in Pulsed Infrared Laser Excited Photothermal Spectroscopy

Stephen E. Bialkowski, *Utah State University*

Accounting for absorption saturation effects in pulsed infrared laser-excited photothermal spectroscopy

Stephen E. Bialkowski

Equations that relate photothermal lens focal lengths and photothermal deflection angles to saturation absorption coefficients are derived. These equations are derived for two-level absorbers with both homogeneously and inhomogeneously broadened transitions. Initial and time-dependent photothermal lens signals are calculated. Equations describing the zero-time signals are exact to within the simplifying assumptions of the derivation, while the time-dependent signals are approximate. The approximation is performed by the use of a finite series of Gaussian functions to model the temperature change profile distorted by nonlinear absorption. The excitation irradiance-dependent signal behavior for rectangular and exponential excitation pulse time profiles for homogeneously and inhomogeneously broadened transitions are compared. Absorbed energies are used to calculate effective absorbances obtained by the use of conventional and photothermal lensing spectrometry. The conclusions drawn from these comparisons are that pulsed laser photothermal spectroscopy is sensitive to the excitation laser's pulse temporal profile and the transition broadening mechanism.

1. Introduction

Nonlinear absorption spectroscopy can yield information about atomic and molecular structures and dynamics that cannot be obtained by conventional spectroscopic techniques.[1] But in addition to the beneficial aspects, nonlinear absorptions measurements can be plagued by experimental artifacts that are difficult to describe and characterize.[2,3] There are several causes of experimental artifacts. First, optical power delivered to the sample with continuous-wave lasers can result in significant sample heating. This heating results in a change in energy-level populations[2,4] and can also cause photothermal lensing. Also, the attenuation varies along the sample pathlength for highly absorbing samples with nonlinear absorption. This gives rise to complicated nonlinear irradiance-dependent absorption behavior.[4] This problem is further complicated if the excitation source also has a spatially varying beam profile.

Among the most successful methods for measuring nonlinear absorption are the pulsed laser photothermal spectroscopy (PL-PTS) techniques.[5] PL-PTS is an ultrasensitive technique used to measure sample absorption. Because of the high sensitivity, samples that are dilute in the absorbing species are utilized. Optically thin samples result in negligible irradiance attenuation through the length of the sample. Nonlinear optical absorption is common in pulsed laser-excited photothermal spectroscopy. Twarowski and Kliger realized the importance of pulsed laser-excited photothermal lens spectroscopy (PL-PLS) for measuring multiphoton transitions.[6,7] The result of their study showed that multiphoton absorption can enhance the PL-PLS signal by narrowing the spatial temperature change profile. Long and Bialkowski[3,8,9] have examined some of the implications of optical saturation in gas-phase infrared PL-PTS. They predicted that saturation of homogeneously broadened transitions flattens the temperature change profile and thereby decreases in the initial, zero-time signal magnitude over that expected.[8] However, optical saturation can actually increase the signal and the precision of the measurements in pulsed laser photothermal deflection spectroscopy (PL-PDS).[2] Multiphoton and optical saturation absorption were observed in infrared PL-PDS of gas-phase chlorofluorocarbon species.[9] However, the excitation energy-dependent signals were used only in terms of their utility for species discrimination. More recently, Poston and Harris[10] estimated saturation irradi-

The author is with the Department of Chemistry and Biochemistry, Utah State University, Logan, Utah 84322-0300.

Received 22 January 1992.
0003-6935/93/183177-13$06.00/0.

ances, energy-transfer kinetics, and enthalpies of triplet benzophenone in condensed-phase samples by examining time-dependent PL-PDS signals over a range of excitation irradiances.

Quantitative information on condensed-phase samples has also come from photothermal wave-mixing techniques. McGraw, *et al.*[11] and Zhu and Harris[12,13] have examined nonlinear absorption in condensed-phase species by using thermal gratings. In this technique a volume phase grating is made by crossing two coherent pump laser beams in the sample. By examining the relative signal powers of the probe laser diffracted through different orders of the distorted grating, nonlinear absorption and kinetic parameters were estimated. The main drawback to this technique is the experimental complexity. Measurements must be made at several probe beam angles in order to extract the information necessary to estimate the nonlinear parameters.

The simplest experiments are those that use a microphone to detect the photoacoustic spectroscopy (PAS) signal generated by the absorbed energy. Cox[14] has measured saturation and multiphoton absorption in SF_6. Chin *et al.*[15] have measured multiphoton absorptions for SF_6 and CH_3OH. Seder and Weitz[16] have measured excitation irradiance-dependent absorption parameters for a number of gas-phase alkyl chlorides and hexadienes. The drawback to the PAS technique is in signal interpretation. The signal is a function of the energy absorbed, the excitation beam profile, and the response of the microphone. Chin *et al.* raised questions over signal interpretation in 1982.[15] There has been substantial progress made in signal interpretation since that time.[16] But the change in the absorbed energy profile over that of the excitation beam profile has not been accounted for in PAS absorption.

The purpose of this study is develop a quantitative theory for irradiance-dependent PL-PTS signals when optical saturation occurs. Although saturation effects are commonly observed, details of how saturation affects the resultant experimental observations have not been previously addressed. These details may be critical to the understanding of how experimental observations can be used to elucidate nonlinear absorption behavior. Equations are derived with the vibrational excitation of gas-phase species in mind. But the results should be applicable to electronic excitation and condensed-phase samples as well.

In infrared laser-excited spectroscopy, calculation of the quantity of light deposited as heat in the sample is difficult owing to the larger number of rotational and vibrational states available to all but the simplest of molecules.[1,2,4] In order to gain some insight into the effects of saturation, this study examines a hypothetical two-level system. The two levels are the specific rovibrational states coupled by excitation radiation. These states are broadened by homogeneous and inhomogeneous mechanisms. Inhomogeneous broadening includes Doppler broadening and the rotational level envelope. Thus rovibrational states not radiatively coupled are treated as background states that make up the inhomogenously broadened line. Two limiting categories of rovibrational energy levels are treated. For small, light molecules, the rovibrational transition spacing is large compared with the homogeneous linewidth, and the transition linewidth is homogeneous. In large molecules, rovibrational transition spacing is small compared with the homogeneous linewidth, although the absorption band is wider than the homogeneous linewidth. In this case the transition is dominated by the inhomogeneous linewidth. If rotational relaxation is slow, the transition linewidth will be strictly inhomogeneous.

Intramolecular energy transfer may be either slow or fast relative to pulsed laser excitation. Treatment of saturation is simplified in either of these two limits. If the background to radiatively coupled state energy-transfer times are long compared with the excitation pulse duration, then individual rovibrational levels, and optical transitions between them, are effectively isolated on the time scale of excitation. If, on the other hand, background to radiatively coupled state energy transfer is fast, then all levels are effectively connected on the time scale of excitation. In this case, inhomogenously broadened transitions are ineffective for isolating individual states. In terms of the dynamics of excitation, the transitions are effectively homogeneous. The latter case is applicable to high-pressure gas and condensed-phase samples.

In PL-PTS, a pulsed excitation laser is used to excit the sample, and a continuous probe laser is used to monitor the refractive-index change that results from sample heating. Sample heating is spatially anisotropic because of the spatially anisotropic pump laser beam profile. The process resulting in the production and decay of the PL-PTS signals can be thought of as occurring in steps. First, pulsed excitation results in the production of excited-state species. The net energy of the sample has increased. Relaxation of excited-state species results in a temperature increase. Relaxation occurs both during excitation and after excitation in the case of long-lived excited states. The temperature increase results in a change of the refractive index. Finally, the temperature returns to that of the surrounding medium by thermal diffusion. There are thus three time-dependent processes: excitation, excited-state relaxation, and thermal diffusion. The time scale for thermal diffusion is generally long compared with either excitation or relaxation.[5]

Spectrometers are designed such that PL-PLS monitors an increase in probe laser beam divergence, and PL-PDS monitors changes in the position of the spatially averaged beam spot. PL-PDS signals are proportional to the off-axis spatial gradient in the refractive index caused by sample heating. The gradient is similar to a prism. PL-PLS signals are proportional to the inverse focal length of the photo-

thermal lens. This lens in turn is related to the on-axis spatial curvature of the refractive-index perturbation caused by spatially dependent sample heating. For an undistorted Gaussian beam profile, refractive-index gradients and curvatures are both proportional to the magnitude of the index perturbation and inversely proportional to the squared excitation laser beam waist radius. When the sample is excited by laser with an undistorted Gaussian beam profile, the two techniques are similar and yield equivalent results.

Central to calculating the PL-PTS signals is a determination of the gradient and the curvature of the spatially dependent refractive-index perturbation. The profile of the absorbed energy is distorted over that of the excitation laser when saturation occurs. The resulting refractive-index perturbations are no longer Gaussian. This results in changes of the gradients and the curvatures that are not necessarily related to each other. In fact, the maximum off-axis gradient increases while the on-axis curvature decreases.

In this paper, equations for PL-PLS and PL-PDS signals at saturating irradiances are derived, and the results are discussed. Two limiting types of saturation behavior are considered. These depend on the particular broadening mechanisms involved in a transition and the relative rates of excitation and relaxation to nonresonant states. The derivations follow the usual order. The spatially dependent energy deposited in the sample during the laser pulse is first calculated. Next the initial PL-PLS and PL-PDS signal magnitudes are found. Finally, the time-dependent signals are calculated. These derivations start with a discussion of optical saturation on the two limiting cases. The usual assumptions applied to PL-PTS are used.[5,6] In particular, the excitation laser beam is Gaussian, the beam waist radius is constant over the length of the sample, and the laser pulse is shorter than the time scale for thermal diffusion.

2. Optical Saturation of Two-Level Transitions

Optical saturation occurs when the stimulated emission rate competes with that of relaxation. In the limit in which dephasing time T_2 is much shorter than either optical pumping or relaxation times T_1, the so-called incoherent system can be treated by coupled rate expressions.[1] The net result is that the optical absorption coefficient can be recast in a form that is dependent on the strength of the excitation source.

The optical frequency-dependent absorption coefficient is given by the convolution of the homogeneous linewidth with the inhomogeneous band shape:

$$\alpha(\nu) = \alpha_0(\nu_0) \int_0^\infty \rho(\nu) g(\nu_0 - \nu) \mathrm{d}\nu, \tag{1}$$

where $\alpha_0(\nu_0)$ (in inverse meters) is the small-signal absorption coefficient at the homogeneous line-band center, $\rho(\nu)$ is the normalized inhomogeneous line-shape function, and $g(\nu_0 - \nu)$ is the Lorentzian line-shape function,

$$g(\nu_0 - \nu) = \frac{\dfrac{1}{(2\pi\tau)^2}}{(\nu_0 - \nu)^2 + \dfrac{1 + E/E_S}{(2\pi\tau)^2}}. \tag{2}$$

The homogeneous linewidth has contributions from both relaxation time τ and power broadening $1 + E/E_S$, where E is the irradiance (in watts per meter squared), and E_S, the saturation irradiance, is defined by

$$E_S = \frac{h\nu_0}{2\sigma(\nu_0)\tau}. \tag{3}$$

The absorption cross section, $\sigma(\nu)$ (in meters squared), is related to the small-signal absorption coefficient by

$$\alpha_0(\nu) = (N_l - N_u)\sigma(\nu), \tag{4}$$

where $N_l - N_u$ is the number density difference (in inverse meters cubed) between lower and upper levels of the transition. Relaxation times used to define the saturation irradiance generally include both T_1 and T_2 processes.[1] However, the rate equations used to derive Eq. (2) are valid only when $T_2 \leq T_1$. In this case relaxation time τ will be that of the limiting kinetic process returning excited-state species to the ground state.

Equation (2) can be integrated for two important limits. For small molecules with rovibrational transition spacing wider than the homogeneous linewidth, the inhomogeneous line shape may be approximated as a delta function at band center ν_0. The exponential absorption coefficient for the homogeneous line is just $\alpha(\nu) = \alpha_0(\nu_0)g(\nu - \nu_0)$, and

$$\alpha(\nu) = \frac{\alpha_0(\nu)}{1 + E/E_S(\nu)}, \tag{5}$$

where $\alpha_0(\nu) = \alpha_0(\nu_0)/[1 + \delta(\nu)]$, $E_S(\nu) = E_S[1 + \delta(\nu)]$, and $\delta(\nu) = [2\pi\tau(\nu - \nu_0)]^2$.

Large molecules have rovibrational transition spacings that are narrower than the homogeneous linewidth, and the absorption is inhomogeneously broadened. By definition, inhomogeneous line broadening means that the molecules exist in several unconnected states. If the time scale for nonresonant state relaxation into the resonant state is shorter than that of excitation to the excited state, every state in the inhomogeneously broadened transition is, in effect, coupled. This results in the depletion of the entire population of lower states by excitation through the resonant state. In other words, the transition is effectively homogeneously broadened since all states are connected on a time scale shorter than that of the excitation. This is a common situation in solution

phase samples[17] and probably occurs in gas-phase samples of moderate pressure.[2]

On the other hand, if the time scales for relaxation into the levels excited by the laser are longer than that of excitation, then the effects of the inhomogeneously broadened transition on the effective saturation absorption coefficient must be taken into account. Thus the second saturation limit is of inhomogeneously broadened transitions with relatively long background state relaxation times. For large molecules with a wide inhomogeneous absorption, the line-shape function is essentially constant over the homogeneous linewidth excited by the narrow-band laser. In this case the irradiance-dependent absorption coefficient is

$$\alpha(\nu) = \frac{\alpha_0(\nu)}{(1 + E/E_S)^{1/2}}, \tag{6}$$

where the inhomogeneous band center absorption coefficient is $\alpha_0(\nu) = \alpha_0(\nu_0)\rho(\nu)/4\tau$.

The inhomogeneous absorption coefficient does not decrease as rapidly with irradiance as the homogeneous one because of the square-root power dependence in the denominator. This effect is due to the increased number of species that can be excited at high irradiances because of power broadening. Thus, although saturation may occur between states with energy differences at or near the excitation energy, i.e., homogeneous saturation, the total number of species excited increases as a result of power broadening of the excitation source linewidth. Inhomogeneous broadening is more likely at lower gas pressures since rotational relaxation is limited by collision rates.

3. Absorbed Energy

In deriving the spatial temperature change profile it is assumed that the radial profile does not change along the axis of propagation of the excitation beam, i.e., the cylindrical symmetry approximation. This assumption is implicit in most derivations of photothermal signals. For this assumption to be valid the sample must be optically thin, and the sample cell length along the axis of propagation must be such that the excitation beam waist does not vary significantly through the cell. The cylindrical symmetry approximation is quite good if the cell length is shorter than the Rayleigh range of the focused beam.

An excitation source propagating in the fundamental TEM_{00} mode has an instantaneous irradiance at radius r from the beam center of

$$E_0(r, t) = \frac{2\Phi(t)}{\pi w^2} \exp\left(\frac{-2r^2}{w^2}\right), \tag{7}$$

where $\Phi(t)$ is the instantaneous radiant power in watts (W), and w is the electric-field beam waist radius parameter. The absorbance law must be modified to include the irradiance-dependent absorption coefficient. The differential expression for the irradiance along sample path z is dependent on the irradiance-dependent absorption coefficient:

$$-\frac{dE_z(r, t)}{dz} = E_z(r, t)\alpha(\nu) = \frac{E_z(r, t)\alpha_0(\nu)}{[1 + E_z(r, t)/E_S]^f}. \tag{8}$$

From Eqs. (5) and (6), exponential factor f is 1 for homogeneously and ½ for inhomogeneously broadened transitions. Use of this factor permits the derivations to be independent of the broadening mechanism. Photothermal spectroscopy is normally performed on samples that are optically thin with respect to absorption. For an optically thin sample, i.e., sample transmission over 99%, the irradiance is essentially constant along the path dz and the $[1 + E_z(r, t)/E_S]^f$ term can be ignored in the integration. This, along with the fact that for small α, $\exp[-\alpha(\nu)l] \approx 1 - \alpha(\nu)l$, results in

$$E_l(r, t) - E_0(r, t) \approx -E_0(r, t)\alpha(\nu)l, \tag{9}$$

where $E_0(r, t)$ is the instantaneous irradiance of the pulsed laser entering the sample, and $E_l(r, t)$ is the irradiance that exits after passing through a sample of path length l. The $\alpha(\nu)$ is one of the saturation absorption coefficients. The amount of heat deposited in the sample per unit volume per pulse is integrated irradiance $U(r)$ (in joules per meter cubed). This is found by integrating the irradiance difference per unit length:

$$U(r) = \int_0^\infty \alpha(\nu)E_0(r, t)dt. \tag{10}$$

Because of the nonlinear irradiance dependence in Eq. (10), the result must be obtained for specific temporal pulse shapes. Constant $E_0(r, t)$ from $t = 0$ to $t = \tau_p$ is a rectangular pulse. This pulse duration may be obtained in electro-optically chopped laser pulses. The energy deposited in the sample over the pulse is

$$U_r(r) = \frac{\alpha_0(\nu)H \exp\left(\frac{-2r^2}{w^2}\right)}{\left[1 + (E/E_s)\exp\left(\frac{-2r^2}{w^2}\right)\right]^f}, \tag{11}$$

where subscript r is used to indicate a rectangular pulse. An average irradiance of $E = 2\Phi(0)/\pi w^2$ (W/m^2), and a time-integrated irradiance of $H = 2\tau_p\Phi(0)/\pi w^2$ (J/m^2) is defined for a rectangular pulse duration of τ_p and a constant radiant power of $\Phi(0)$.

Another important case is an exponential temporal profile that may be used in order to resemble more closely the output of transverse discharged lasers such as transversely excited atmospheric CO_2 and the excimers. In this case,

$$\Phi(t) = \Phi(0)\exp(-t/\tau_p). \tag{12}$$

The exponentially averaged power is $\Phi(0) = Q/\tau_p$,

where Q is the total pusle energy (in joules). The energies absorbed by the sample are

$$U_e(r) = \alpha_0(\nu)E_S\tau_p \ln\left[1 + (E/E_S)\exp\left(\frac{-2r^2}{w^2}\right)\right] \quad (13)$$

for homogeneously broadened transitions and

$$U_e(r) = 2\alpha_0(\nu)E_S\tau_p\left\{\left[1 + (E/E_S)\exp\left(\frac{-2r^2}{w^2}\right)\right]^{1/2} - 1\right\} \quad (14)$$

for inhomogeneously broadened transitions. Because the irradiance varies with time for the exponential pulse, an average irradiance is defined as $E = 2Q/\tau_p\pi w^2$.

4. Initial Deflection Angles and Focal Lengths

The initial PL-PDS and PL-PLS signals are those occurring shortly after pulsed laser excitation and relaxation of those species remaining in the excited state but before thermal diffusion of excess thermal energy away from the region excited by the pulsed laser. For a thermal diffusion time constant τ_c that is much greater than either τ_p or the time required for excited-state energy relaxation, radial-dependent temperature change $\delta T(r)$ is simply absorbed energy $U(r)$ divided by the heat capacity of the sample. This is generally a valid assumption since τ_c are typically of the order of milliseconds.[5] Finite signal rise times that are due to excited-state species that relax after the excitation pulse can be observed in certain cases. But the heat capacity approximation still holds as long as the time required for the maximum signals to develop is much shorter than that of the thermal decay. Thus, although the maximum signal may take a finite amount of time to develop, the maximum temperature change is still approximated well by the absorbed energy divided by the heat capacity. Initial temperature changes for saturation absorption are shown in Table 1.

PL-PTS signals are generated as a direct consequence of the spatially dependent refractive-index perturbations that arise because of sample heating. The PL-DPS signal is proportional to the deflection angle and the PL-PLS signal is related to the inverse focal length of the thermal lens.[5,6] These elements are calculated from the refractive-index gradient and the second spatial derivative of the index for PL-PDS and PL-PLS, respectively. The refractive-index change usually occurs only because of a change in sample density. Sample density is in turn related to the temperature change at constant pressure. The density-dependent refractive-index change and the temperature-dependent density change are combined into a temperature-dependent refractive-index change. Temperature is found from the absorbed energy and the heat capacity of the sample, and the initial signal is taken to be the maximum signal that occurs before thermal decay.

In the limit of small probe ray path perturbations, the deflection angle and inverse focal lengths are[3,5]

$$\phi = \frac{l}{n_0\rho C_P}\left(\frac{dn}{dT}\right)_P \frac{d}{dr}U(r), \quad (18)$$

$$F^{-1} = \frac{-l}{n_0\rho C_P}\left(\frac{dn}{dT}\right)_P \left|\frac{d^2}{dr^2}U(r)\right|_{r=0}, \quad (19)$$

respectively. In these equations n_0 is the refractive index of the sample, ρC_P is the heat capacity made up of density ρ and specific heat capacity C_P, and $(dn/dT)_P$ is the change in the refractive index with a change in temperature at constant pressure.

The deflection angle and thus the PL-PDS signal change with radial offset from the pump laser beam center. The equation for calculating the energy-dependent PL-PDS used here is

$$\phi = \frac{l}{n_0\rho C_P}\left(\frac{dn}{dT}\right)_P \left|\frac{d^2}{dr^2}U(r)\right|_{r=w/2} \quad (20)$$

since, in the absence of saturation, the photothermal deflection signal is a maximum when the probe laser is offset by half of the pump laser electric-field beam waist radius. The deflection angles for rectangular pulse excitation are

$$\phi_r = \frac{-1}{n_0}\left(\frac{dn}{dT}\right)_P \frac{2\alpha_0(\nu)lH}{w\rho C_P} \times \frac{\exp(f/2)[1 + \exp(-1/2)(1 - f)E/E_S]}{[\exp(1/2) + E/E_S]^{f+1}}. \quad (21)$$

The inverse focal length of the simple thermal lens is calculated by the use of Eq. (12) in Eq. (20):

$$F_r^{-1} = \frac{1}{n_0}\left(\frac{dn}{dT}\right)_P \frac{4\alpha_0(\nu)lH}{w^2\rho C_P} \frac{1 + (1 - f)E/E_S}{(1 + E/E_S)^{f+1}}. \quad (22)$$

For the exponential shaped excitation laser pulse the initial deflection angle for a probe beam offset of $r = w/2$ is

$$\phi_e = \frac{-1}{n_0}\left(\frac{dn}{dT}\right)_P \frac{2\alpha_0(\nu)lH}{w\rho C_P} \frac{\exp(-1/2)}{[1 + \exp(-1/2)E/E_S]^f}. \quad (23)$$

Table 1. Temperature Changes for Saturation Absorption

Rectangular pulse

$$\delta T_r(r) = [\alpha_0(\nu)H/\rho C_P]\exp(-2r^2/w^2)[1 + (E/E_S)\exp(-2r^2/w^2)]^{-f} \quad (15)$$

Exponential pulse, homogeneous line

$$\delta T_e(r) = [\alpha_0(\nu)E_S\tau_P/\rho C_P]\ln[1 + (E/E_S)\exp(-2r^2/w^2)] \quad (16)$$

Exponential pulse, inhomogeneous line

$$\delta T_e(r) = [2\alpha_0(\nu)E_S\tau_p/\rho C_P][[1 + (E/E_S)\exp(-2r^2/w^2)]^{1/2} - 1\} \quad (17)$$

The inverse focal length is

$$F_e^{-1} = \frac{1}{n_0}\left(\frac{dn}{dT}\right)_P \frac{4\alpha_0(\nu)lH}{w^2\rho C_P}\frac{1}{(1 + E/E_S)^f}. \quad (24)$$

The integrated irradiance $H = E\tau_p$ is defined for exponential pulse expressions.

5. Time-Dependent Signals

The time-dependent behavior of the photothermal deflection angles and focal lengths is found by solving the thermal diffusion equation for the absorbed irradiance. Time-dependent PL-PDS and PL-PLS signals are relatively easy to derive for initial absorbed irradiance profiles that are Gaussian in form. Solutions to the diffusion equation can be found by integration over the Green's function for a radially symmetric source or by transform techniques. But analytical solutions for the time-dependent signals are not known in cases in which saturation distorts the initial Gaussian profile. These time-dependent signals can be approximated by first finding a set of Gaussians that, when superimposed, accurately describe the initial spatially absorbed irradiance profile. The heat transfer law is additive with respect to the thermal sources. Thus the individual Gaussian profiles in the superposition approximation can be treated as a separate heat source. The time-dependent signal is then the sum of the time-dependent signals from each of the component Gaussian heat sources.

The thermal diffusion equation,

$$\frac{d}{dt}\delta T(x, y, z, t) = K\nabla^2\delta T(x, y, z, t) + \theta(x, y, z, t), \quad (25)$$

where K is the thermal diffusion coefficient, and θ is the time rate of temperature change of the source, is solved for a cylindrically symmetric source in an isotropic medium and has a solution[5]

$$\delta T(r, t) = \int_0^t dt' \int_0^\infty G(r, r', t')dr'. \quad (26)$$

The Green's function, $G(r, r', t')$, for the Gaussian source is

$$G(r, r', t') = \frac{r'Q'(r', t')}{2\rho C_P K t'}\exp\left[\frac{-(r^2 + r'^2)}{4Kt'}\right]I_0\left(\frac{rr'}{2Kt'}\right), \quad (27)$$

where $Q'(r', t)$ is the time rate of heat release and $I_0(\,)$ is the modified zero-order Bessel's function. Integration over time is performed first. Since the rate of heat release is assumed to be much faster than thermal diffusion the time integral over any fast excitation will appear as a delta function on the time scale of the thermal decay. $Q'(r, t)$ is just $U(r, t)\delta(t)$ and

$$\delta T(r, t) = \frac{1}{2Kt}\int_0^\infty \delta T(r')\exp\left[\frac{-(r^2 + r'^2)}{4Kt}\right]I_0\left(\frac{rr'}{2Kt}\right)r'dr'. \quad (28)$$

Integration can be performed if $\delta T(r)$ can be expanded as a series of N Gaussian exponents:

$$\delta T(r) = \sum_{k=1}^{N} a_k \exp\left[\frac{-kr^2}{w^2}\right]. \quad (29)$$

The time-dependent temperature change profile is then

$$\delta T(r, t) = \sum_{k=1}^{N}\frac{a_k}{1 + kt/\tau_c}\exp\left[\frac{-kr^2}{w^2(1 + kt/\tau_c)}\right], \quad (30)$$

where $\tau_c = w^2/4K$ is the characteristic thermal decay time. The PL-PDS signal with a probe beam offset at radius $r = w/2$ is

$$\phi(t) = -\frac{2l}{wn_0}\left(\frac{dn}{dT}\right)_P\sum_{k=1}^{N}\frac{ka_k}{(1 + kt/\tau_c)}\exp\left[\frac{-k}{2(1 + kt/\tau_c)}\right], \quad (31)$$

and the PL-PLS signal is

$$F^{-1}(t) = \frac{4l}{w^2n_0}\left(\frac{dn}{dT}\right)_P\sum_{k=1}^{N}\frac{ka_k}{(1 + kt/\tau_c)^2}. \quad (32)$$

Expansion coefficients a_k are found by linear regression. Ten terms are usually adequate to model the initial temperature change profile to a high degree of accuracy. Accuracy is checked by inspection of the χ^2 parameter of the regression. Different models, i.e., the use of different exponential dependencies of the basis Gaussian functions, give similar results.

6. Discussion

A. Initial Temperature Change Profiles

Equations that describe the initial radially dependent temperature change profile for the four different cases involving homogeneously and inhomogeneously broadened transitions excited with rectangular and exponential pulses appear to be quite different. However, all cases have the same low irradiance limit. For irradiances that are much less than those required for saturation, the temperature change results all converge to

$$\lim_{\Phi_0\to 0}\delta T(r) = \frac{\alpha_0(\nu)H}{\rho C_P}\exp\left(\frac{-2r^2}{w^2}\right). \quad (33)$$

As expected, all cases converge to the same spatial form, that of the excitation laser beam profile, when saturation is not occurring.

When the excitation irradiance approaches or ex-

ceeds that required for saturation, the initial spatial temperature change profile becomes distorted from that of the excitation laser profile. Radially dependent initial temperature change profiles for several different saturation and excitation pulse types are illustrated in Figs. 1–3. The homogeneously broadened transition excited with a rectangular temporal pulse, illustrated in Fig. 1, has the most marked change in the temperature change profile with respect to irradiance. As E exceeds E_S, the top of the profile becomes flatter because of saturation near the beam center, where the irradiance is highest. This behavior will result in a decreased thermal lens signal at irradiances in excess of E_S since this signal is proportional to the second derivative with respect to radius. In fact, the limiting temperature change is

$$\lim_{\Phi_0 \to \infty} \delta T_r(r) \approx \frac{\alpha_0(\nu)\tau_p E_S}{\rho C_P}. \tag{34}$$

Since the high irradiance-limited temperature change is independent of radius, there will be no initial PL-PLS signal. But there is a temperature increase. The profile of the temperature increase will change with time as a consequence of thermal diffusion. The radial diffusion process is Gaussian, and a finite PL-PLS signal will develop over time. This behavior is shown below.

The difference between the exponential pulse temperature change and that of the rectangular pulse is significant for a homogeneously broadened transitions. The spatial profile of the thermal perturbation for a homogeneously broadened transition being excited with an exponential shaped temporal profile is illustrated in Fig. 2. For exponential pulse excitation, the radially dependent on-axis temperature change for irradiances far in excess of that for saturation is

$$\lim_{\Phi_0 \to \infty} \delta T_e(r) \approx \frac{\alpha_0(\nu)\tau_p E_S}{\rho C_P}\left[\ln(E/E_S) - \frac{2r^2}{w^2}\right] \tag{35}$$

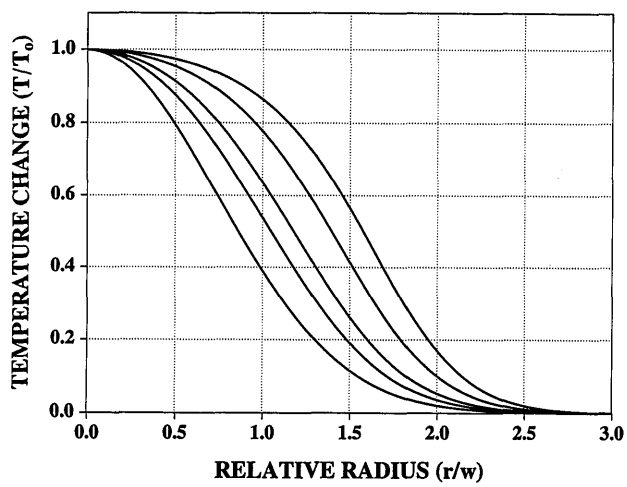

Fig. 1. Plot of the scaled temperature change profiles for a homogeneously broadened transition by a rectangular pulsed excitation. The profiles correspond to E/E_S's of 0.1, 1, 2, 5, and 10, from the narrowest to the widest.

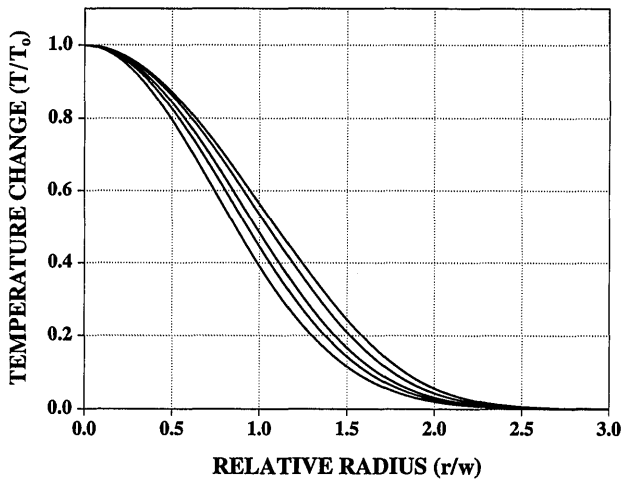

Fig. 2. Plot of the scaled temperature change profiles for homogeneously broadened transition excited with an exponential pulse with E/E_S's of 0.1, 1, 2, 5, and 10, from the narrowest to the widest.

for a homogeneously broadened transition. Since the radial dependence becomes isolated from the irradiance in this limit, the PL-PLS signal strength will reach a maximum value that is independent of excitation irradiance. This can be seen by taking the second derivative of the limiting profile in approximation (35):

$$\frac{d^2}{dr^2}\left[\lim_{\Phi_0 \to \infty} \delta T_e(r)\right] \approx -\frac{4\alpha_0(\nu)\tau_p E_S}{w^2 \rho C_P}. \tag{36}$$

In this limit the PL-PLS signal depends on only the number density of molecules and the excited-state relaxation time constant since $\alpha_0(\nu) \approx N_{tot}\sigma(\nu)$ and $E_S = h\nu/2\sigma(\nu)\tau$. This feature of optical saturation could be used to increase the accuracy of the PL-PLS experiment. In this limit, the signal would not have to be corrected for pulsed laser irradiance variations

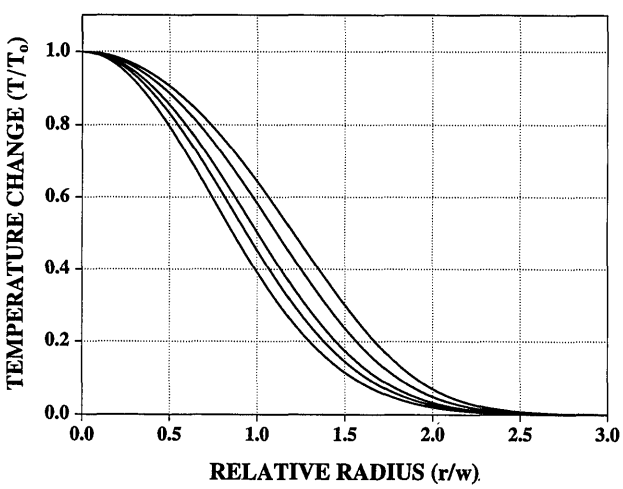

Fig. 3. Plot of the scaled temperature change profiles for an inhomogeneously broadened transition by a rectangular pulse for E/E_S's of 0.1, 1, 2, 5, and 10, from the narrowest to the widest.

in order to obtain the sample absorbance or analyte concentration.

Differences in the radially dependent temperature changes of homogeneously broadened transitions for rectangular and exponential pulse shapes can be seen by examining Fig. 1 and 2. The fact that different temporal pulse shapes influence the radial dependence of the temperature change indicates that the experimental determination of saturation behavior must be performed with well-characterized pulses.

Rectangular pulse excitation of inhomogeneously broadened transitions results in temperature change profiles that do not flatten with increasing irradiance. Initial spatial profiles for inhomogeneously broadened saturation are shown in Fig. 3. The limiting temperature change profiles in this case are

$$\lim_{\Phi_0\to\infty} \delta T_r(r) \approx \frac{\alpha_0(\nu)\tau_p}{\rho C_P}(EE_S)^{1/2}\exp(-r^2/w^2). \quad (37)$$

The radial dependence has changed but is still Gaussian in form. As indicated by the temperature change profiles in Table 1, inhomogeneously broadened transitions will always have an initial, on-axis curvature. Because the diffusion process broadens a Gaussian, this will result in a PL-PLS signal that is a maximum at zero time. The radius of the initial temperature change effectively increases by a factor of $\sqrt{2}$ in the high irradiance saturation limit.

The limiting spatial profile of thermal perturbation for an inhomogeneously broadened transition being excited with an exponential shaped temporal profile is

$$\lim_{\Phi_0\to\infty} \delta T_e(r) \approx \frac{2\alpha_0(\nu)\tau_p}{\rho C_P}(EE_S)^{1/2}\exp(-r^2/w^2). \quad (38)$$

The form of this limiting profile is the same as that which would be obtained with the rectangular pulse. But there is a factor of 2 difference in the magnitude. The factor of 2 may be due to the different way the irradiance is defined for rectangular and exponential pulses. The form of the radially dependent temperature change is nearly identical to that shown in Fig. 3. In both cases the resulting temperature change profile is a Gaussian with the same radial width. Thus the temperature change profile is apparently not dependent on pulse shape for inhomogeneously broadened transitions.

B. Irradiance-Dependent Initial Time PL-PTS Signals

Measurements of zero-time signals as functions of excitation irradiance may yield the most definitive information regarding the character of the transition. Zero-time PL-PLS signals are plotted in Fig. 4. The four conditions discussed above are shown. The top two curves correspond to inhomogeneous transitions with exponential and rectangular pulse excitations. The bottom two are for homogeneously broadened transitions excited with exponential and rectangular pulses. In all cases the signals are scaled to unit $\alpha_0(\nu)l/n_0w^2\rho C_P$ and $(dn/dT)_P$.

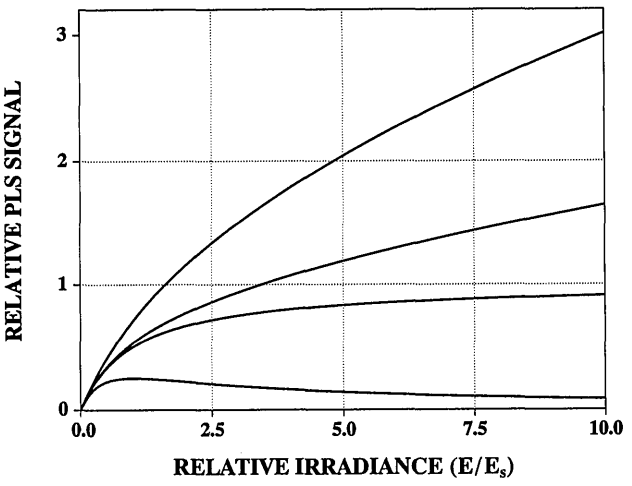

Fig. 4. Irradiance-dependent zero-time PL-PLS signals. Curves, from top to bottom: inhomogeneous exponential pulse, inhomogeneous rectangular pulse, homogeneous exponential pulse, homogeneous rectangular pulse.

The zero-time PL-PLS signal for the case of rectangular pulse excitation of a homogeneously broadened transition exhibits an initial increase in signal followed by a decrease in signal with increasing irradiance. This behavior is due to flattening of the initial temperature change profile at high irradiances. The homogeneously broadened transitions will have zero-time temperature change profiles that are dependent on the particular temporal pulse profile. Since the inverse focal length depends on the zero-time temperature change profiles through the second radial derivative, the PL-PLS signals should also be dependent on the pulse temporal profile. In fact, a rectangular pulse results in a limiting, i.e., high irradiance, zero-time PL-PLS signal that is zero. On the other hand, the limiting signal is constant and independent of irradiance when an exponential pulse is used. These trends can be seen by examining Fig. 4. The exponential pulse zero-time PL-PLS signal has reached a constant value at an E/E_S of 10, while the rectangular pulse signal is still decreasing at this relative irradiance.

The main difference between the irradiance-dependent PL-PLS signals for the inhomogeneously broadened transitions with exponential and rectangular pulse shapes is the factor of two difference in magnitude. The shapes of these two irradiance-dependent signals are essentially the same. They are indistinguishable when scaled and replotted. On the other hand, the shapes of the homogeneously broadened cases show that differences in the temporal profile of the pulse result in large differences in the irradiance-dependent signals.

These combined features could be used to determine whether a transition was homogeneously or inhomogeneously broadened if one has control over the temporal laser pulse shape. Irradiance-dependent signals are relatively independent of excitation pulse time dependence for the inhomogeneously broadened case but are dependent on the pulse shape

in the case of the homogeneously broadened transition. So an experiment comparing the irradiance-dependent zero-time signals for two or more laser pulse shapes would allow one to determine whether the transition is homogeneously or inhomogeneously broadened.

There are significant differences in the shapes of the irradiance-dependent zero-time signal curves for a particular laser pulse shape but with different broadening mechanisms. Thus, with the use of a particular laser, the mechanism may be elucidated by examining the shape of the irradiance-dependent zero-time PL-PLS signals. In particular, homogeneously broadened transitions have irradiance-dependent zero-time PL-PLS signals that either decrease or stop increasing with increasing irradiance. Inhomogeneously broadened transitions have irradiance-dependent PL-PLS signals that increase with increasing irradiance past saturation.

The equations describing the PL-PDS signals are similar to those for PL-PLS. The time- and irradiance-dependent signals are nearly equivalent for the conditions used to derive the equations. But PL-PDS introduces another degree of freedom, that of the pump–probe laser beam offset. This extra degree of freedom means that additional measurements must be made if the signals are to be used for the quantitative measurement of nonlinear effects. Measuring the exact pump–probe laser beam offset is difficult, and attempting to adjust the offset by maximizing the signal when saturation is occurring is bound to be problematic since the offset to the maximum gradient changes with the degree of saturation. One solution is to adjust the pump–probe laser beam offset for maximum signal when saturation is not occurring. In the Fourier law of diffusive heat transfer, the temperature diffusion rate is proportional to the gradient. Thermal diffusion occurs in a direction such as to decrease this gradient. Consequently, the maximum gradient must occur at zero time, and thermal diffusion can only decrease this maximum gradient. Thus the deflection angle that is due to the maximum gradient must also decrease with time. On the other hand, time-dependent gradients at locations other than that where the maximum initial gradient occurs may increase in time in cases in which E exceeds E_S. Subsequently, a range of time-dependent PL-PDS signals should be observed as the pump–probe beam offset is changed when the irradiance exceeds E_S. The potential measurement problems associated with the interpretation of the time domain PL-PDS signal would lead one to conclude the PL-PLS is better suited for photothermal studies when optical saturation occurs.

However, even with these potential measurement problems, PL-PDS has a potential application in quantitative analysis. Optical saturation ultimately limits conventional absorption spectrophotometry. Optical saturation, along with shot-noise statistics, has been used to calculate ultimate limits of detection in analytical spectroscopy.[18] PL-PDS can circumvent these limits both by the use of an indirect measure of optical absorbance, thereby circumventing the shot-noise limitation, and by producing a signal that increases with irradiances well beyond those required for saturation.[3] As seen in Fig. 1, there is an increase in the slope of the scaled temperature change profiles with increasing irradiance. However, increasing the irradiance also increases the radial offset to the maximum gradient. Thus the location of the maximum gradient changes in space as a function of the degree of saturation. Subsequently, in order to benefit from the larger signals produced by the increased gradients under saturation conditions, the probe beam must be offset to the maximum gradient position. This may be accomplished if the PL-PDS signal is maximized by adjusting the pump–probe laser offset for a species that is being saturated.

Maximum zero-time PL-PDS signals can be obtained from the first derivative of the temperature change profiles by finding the radial pump–probe laser offset that maximizes the deflection angle.[3] In the case of inhomogeneously broadened transitions, the limiting temperature change Gaussian radius is $\sqrt{2}$ wider than that of the pump laser. Thus the optimum pump–probe laser offset for irradiance far in excess of that required for saturation would be $r = w/\sqrt{2}$. Analytical expressions for the PL-PDS signals can be found in this case. Such is not the case for homogeneously broadened transitions. In that case the offset to the radius of the maximum gradient increases with increasing irradiance.

Maximum zero-time PL-PDS signals are illustrated in Fig. 5. These were calculated by finding the pump–probe laser offset that maximized the PL-PDS for each relative irradiance. In contrast to the PL-PLS signals illustrated in Fig. 4, all PL-PDS signals increase with increasing irradiance. There are only minor differences between PLS and PDS signals for

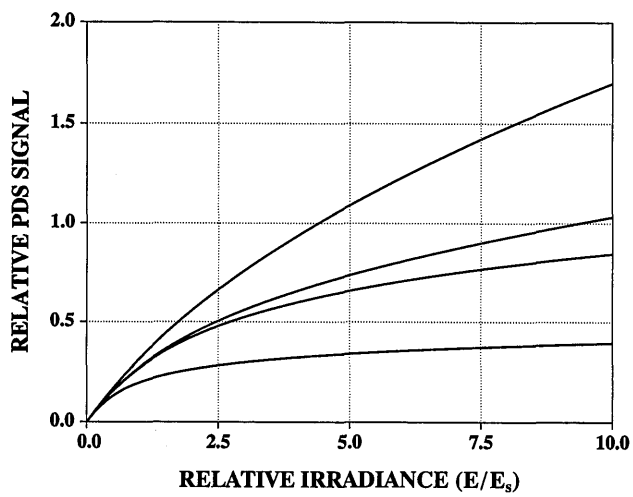

Fig.5. Irradiance-dependent zero-time PL-PDS signals for which the pump–probe laser beam offset was adjusted to maximize the signals. Curves, from top to bottom: inhomogeneous exponential pulse, inhomogeneous rectangular pulse, homogeneous exponential pulse, homogeneous rectangular pulse.

the inhomogeneously broadened transitions. But PL-PDS signals produced for the homogeneously broadened transitions show enhanced signals and sensitivities at higher irradiance. The exponential pulse case does not level off, and the rectangular pulse case does not decrease, with increasing irradiance, as was the case for PLS.

C. Time-Dependent PL-PLS Signals

It is interesting to examine the time dependencies of the PL-PLS signals as functions of excitation irradiance, pulse shape, and type of transition broadening. The PL-PDS signals from Eq. (31) will behave in a similar fashion, and only the PL-PLS signals are discussed below. Figures 6–8 show time-dependent signals for saturation of homogeneously and inhomogeneously broadened transitions with rectangular and exponential pulses. These time-dependent signals were calculated with the temperature change profiles given in Table 1. Linear combination coefficients for the initial temperature change profile were found by conventional linear regression. Some distortion in the early time signal observed in Fig. 6 for $E/E_S = 10$ may be due to a lack of accuracy of the 10-term series for high irradiance profiles.

Figure 6 is particularly interesting in that it illustrates that, while the zero-time inverse focal length decreases with increasing irradiance past the saturation irradiance, the PL-PLS signal increases with time even after the initial onset. The increase in the PL-PLS signal is due to the Gaussian nature of thermal diffusion for cylindrical symmetric sources. When the initial temperature change profile is flattened, like that of a top hat profile, thermal diffusion serves to increase the curvature of the temperature change, thereby causing the PL-PLS signal to increase with time.

On the other hand, Figs. 7 and 8 exhibit monotonic thermal decay behavior. Plots in which the time-dependent signal decays are scaled to the same height reveal that the thermal decay characteristics are only mildly altered by saturation. For the inhomogeneous transition case shown in Fig. 7, the temperature change profile radius changes by a factor of $\sqrt{2}$ going from low to high irradiance. Since $\tau_c = 4K/w^2$, a factor of 2 increase in the characteristic decay time is expected at limiting irradiances. Exponential pulse excitation of inhomogeneously broadened transition results in temporal behavior that is similar to that shown in Fig. 7. This is expected since, as discussed above, the high and low irradiance-limited temperature change profiles are the same for rectangular and exponential pulse excitations of inhomogeneous transitions.

Figure 8 shows some distortion from the monotonic decay behavior above E/E_S of 5 for exponential pulse excited homogeneous saturation. The reason for this is not clear. But it is probably due to the

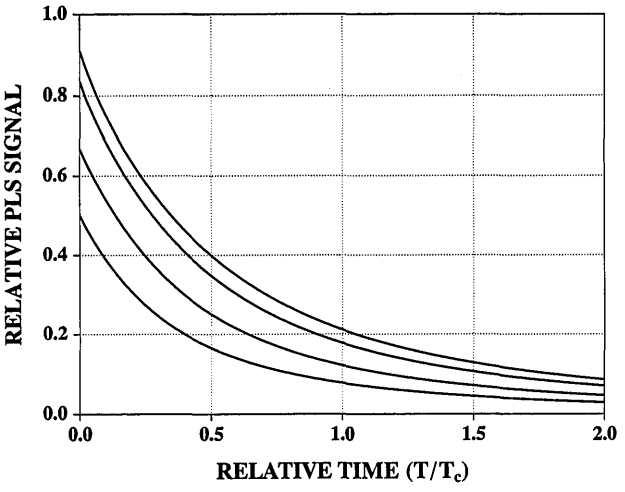

Fig. 7. Time-dependent PL-PLS signals for a rectangular pulse excitation of a inhomogeneously broadened transition for E/E_S's of 1, 2, 5, and 10. The maximum signal increases with irradiance.

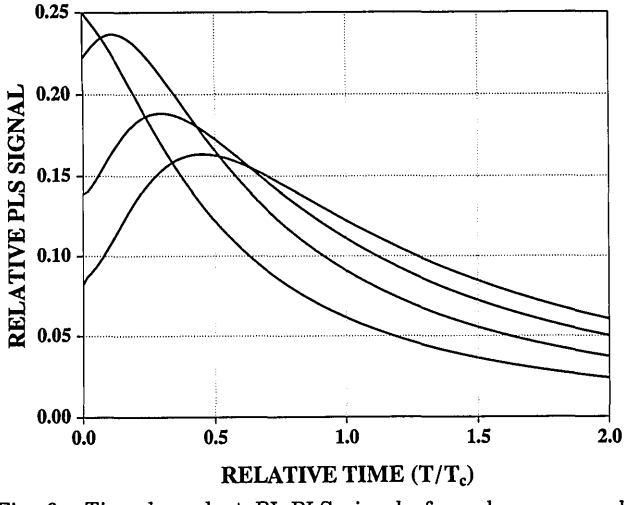

Fig. 6. Time-dependent PL-PLS signals for a homogeneously broadened transition and rectangular pulse excitation. The E/E_S's are 1, 2, 5, and 10, with the maximum PLS signal decreasing with irradiance.

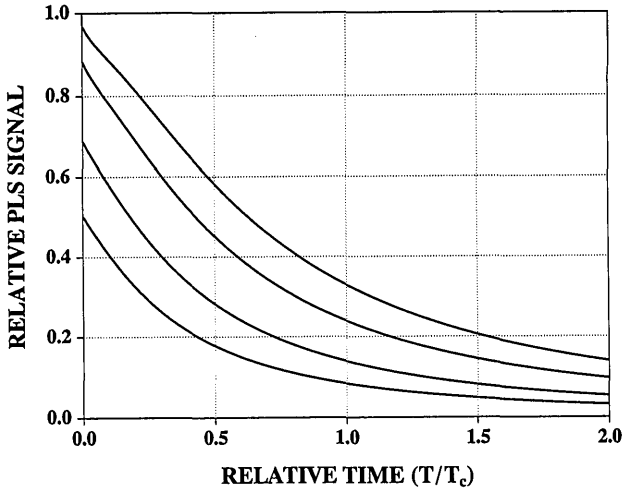

Fig. 8. Time-dependent PL-PLS signal for an exponential pulse excitation of a homogeneously broadened transition for E/E_S's of 1, 2, 5, and 10. The maximum signal increases with irradiance.

non-Gaussian nature of the initial temperature change distribution.

There are two points to be made after comparing Figs. 6–8. First, exponential shaped laser pulse excitation results in time-dependent PL-PLS signals at which the maximum signal occurs promptly after the initial thermal relaxation of the excited state. This reduces the requirement of measuring the time-dependent signals at several irradiances in order to determine the maximum signal magnitude accurately. The energy-dependent zero-time signals discussed below contain more information than the time-dependent decays. There are only minor changes in the thermal decay portion of the data. The second point is that rectangular pulse excitation of the homogeneously broadened transition shows a signal increase that could be mistaken for an apparent slow heat release in the relaxation kinetics. Signals exhibiting similar slow heat release have been observed in PL-PTS.[13] But by varying quencher concentrations, these transients were found to be due to relaxation kinetics.

The question remains as to whether experimental evidence can be used to discern the two limiting saturation conditions. The time-dependent signals shown in Figs. 6 and 7 for rectangular pulse excitation are dramatically different. But, experimentally, rectangular pulses are more difficult to obtain. The exponential pulse excited inhomogeneous saturation temporal response is similar to that caused by rectangular pulse excitation. Thus time-dependent signals are not sensitive enough to discriminate between homogeneous and inhomogeneous line-broadening mechanisms for exponential shaped pulse lasers. On the other hand, the irradiance-dependent, zero-time PL-PLS signal behavior in Fig. 4 is quite different for homogeneous and inhomogeneous cases with a particular laser pulse shape. These measurements are readily obtained and are apparently more sensitive to changes in the nonlinear absorption characteristics.

D. Volume-Integrated Energy and Comparison of Absorption Spetrophotometry with Photothermal Spectrometry

The absorbed energies can be used to predict the effective absorbance that would be measured by absorption spectrophotometry. In the latter, the ratio of absorbed to incident energy is calculated in the optically thin limit. The volume-integrated absorbed energy is obtained from

$$Q_{abs} = 2\pi l \int_0^\infty U(r) r dr, \tag{39}$$

which, for rectangular pulse excitation, yields

$$Q_r = 2\pi l \alpha \tau_p E_S (w^2/4) \ln(E/E_S + 1) \tag{40}$$

for homogeneously broadened transitions, and

$$Q_r = 4\pi/\alpha \tau_p E_S (w^2/4)[(E/E_S + 1)^{1/2} - 1] \tag{41}$$

for inhomogenously broadened transitions. The relative absorbance for optically thin samples is $A = \log_{10}(1 - Q_{abs}/Q_{tot}) \approx -2.303\, Q_{abs}/Q_{tot}$. Relative absorbances from these equations are illustrated in Fig. 9. The upper trace indicates the effective absorbance that is due to inhomogeneously broadened transitions and the lower indicates the absorbance that is due to homogeneously broadened transitions. Both traces are scaled to a maximum relative absorbance of 1. Normally the saturation irradiance is defined as that irradiance at which the absorbance decreases to half the small-signal value for a homogeneously broadened transition. The reason why the effective absorbance decreases to half the small-signal value at a relative irradiance greater than 1 is due to the Gaussian shaped beam profile. A similar effective absorbance could be obtained by the use of photoacoustic spectroscopy if the change in the radius of the temperature change profile did not significantly affect acoustic wave generation.

For analytical utility, absorbances are also calculated from the PL-PTS signals. This is accomplished by dividing the PL-PLS signal by the excitation energy. Absolute absorption coefficients are typically determined by standardization with an analyte of known absorbance. The relative absorbances found for zero-time PL-PLS are illustrated in Fig. 10. Again, the upper trace is due to inhomogeneously broadened transitions and the lower trace is due to homogeneously broadened transitions; the results for rectangular pulse excitation were used.

A comparison of the absorption spectrometry results in Fig. 9 with those obtained by PL-PLS in Fig. 10 indicates that the error associated with the use of PL-PLS to measure absorbance is greater than that associated with conventional techniques when saturation is occurring. An error would arise only if it was not known that saturation was occurring. On the other hand, signal measurement is intrinsically more precise with PL-PLS because of the indirect nature of signal measurement.[18] In absorption spectrophotom-

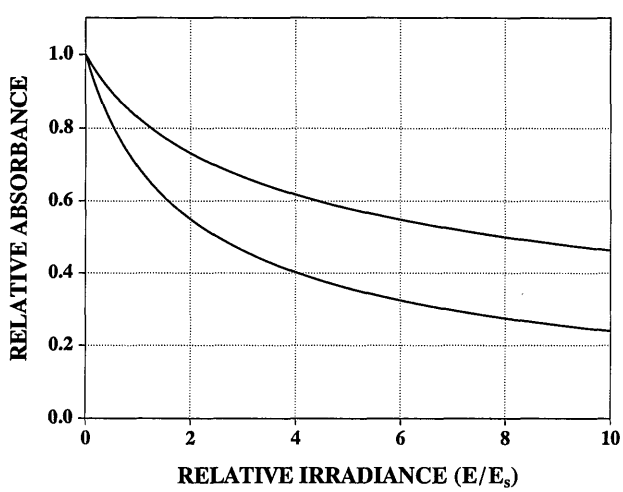

Fig. 9. Relative spectrophotometric absorbance for homogeneously (lower trace) and inhomogeneously (upper trace) broadened transitions by rectangular pulse excitation.

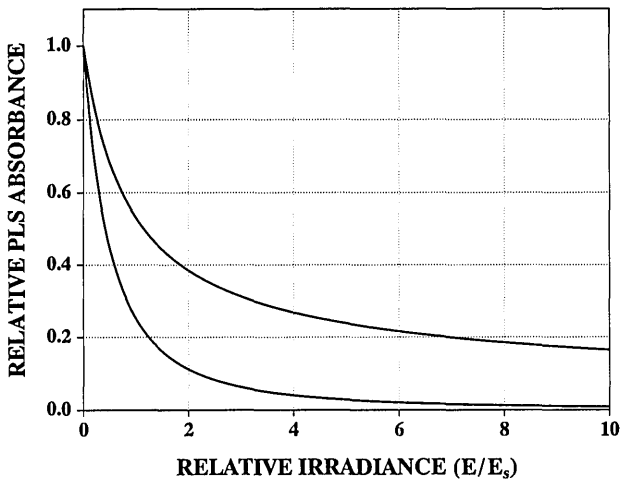

Fig. 10. Relative absorbances determined by PL-PLS spectrometry for homogeneously (lower trace) and inhomogeneously (upper trace) broadened transitions with rectangular pulse excitation.

etry of optically thin samples the absorbance is calculated from the relatively small change in transmitted energy. Since shot noise ultimately limits the minimum change that can be detected, decreases in the relative absorbance decrease the measurement precision. On the other hand, PL-PLS signals for inhomogeneously broadened transitions and maximum PL-PDS signals have analytical signals that increase with increasing irradiance beyond that required for saturation. Thus the precision of PL-PTS absorbance measurements are greater than those of absorption spectrophotometry. In order to avoid errors in calculated absorbance when PL-PTS is used, the PL-PTS signal could be measured as a function of the excitation irradiance. Examination of these data for nonlinear behavior would reveal saturation effects, and the relative absorbance data could be extrapolated to the small-signal absorbance.

7. Conclusions

The equations describing excitation irradiance and time-dependent PL-PTS signals have been derived for the ideal case of two-level absorption. The equations show that PL-PTS signals are sensitive to both the type of transition broadening and to the temporal profile of the pulse laser. PL-PTS signals exhibit behavior that is only indirectly related to the simple saturation absorption equations shown in Eqs. (5) and (6). Thus nonlinear energy-dependent signals alone cannot be used to interpret the nonlinear absorption behavior directly. PL-PTS signals must be interpreted in the light of equations that take into account the spatial and temporal variations of the thermal perturbation.

PL-PDS has a signal magnitude advantage over PL-PLS when optical saturation occurs. This is due to the fact that the probe laser beam may be offset to the position of the maximum refractive-index gradient. But PL-PLS is favored in terms of accuracy. The probe laser beam offset of PL-PDS must be measured in order to obtain accurate results. Relative beam position measurement is difficult and prone to errors that would decrease the accuracy of the analysis.

The temporal rise time of the PL-PLS signal can be affected when optical saturation occurs. This distortion could be mistaken for energy-transfer kinetics.

Finally, when used to calculate absorbance, PL-PLS introduces more errors compared with absorption spectrophotometry or photoacoustic spectrometry. But the precision of indirect absorption measurements is higher than that of spectrophotometry. Since photoacoustic spectrometry is an indirect measurement technique that is responsive to the total amount of heat absorbed, this technique may be ideal for optical absorption measurements of samples that saturate. In any case, absorbance measurement errors can be avoided by examination of the irradiance-dependent signals.

This research was funded in part by the National Science Foundation, CHE-9005769.

References

1. J. I. Steinfeld, *Molecules and Radiation: An Introduction to Modern Molecular Spectroscopy,* 2nd ed. (MIT, Cambridge, Mass., 1985).
2. O. R. Wood, P. L. Gordon, and S. E. Schwartz, "Saturation of infrared absorption in gaseous molecular systems," IEEE J. Quantum Electron. **QE-5,** 502–513 (1969).
3. G. R. Long and S. E. Bialkowski, "Saturation effects in gas phase photothermal deflection spectrophotometry," Anal. Chem. **57,** 1079–1083 (1985).
4. I. Burak, J. I. Steinfeld, and D. G. Sutton, "Infrared saturation in sulfur hexafluoride," J. Quant. Spectrosc. Radiat. Transfer **9,** 959–980 (1969).
5. J. A. Sell, ed., *Photothermal Investigations of Solids and Fluids,* (Academic, New York, 1989).
6. A. J. Twarowski and D. S. Kliger, "Multiphoton absorption spectra using thermal blooming," Chem. Phys. **20,** 253–258 (1977).
7. A. J. Twarowski and D. S. Kliger, "Multiphoton absorption spectra using thermal blooming II. Two-photon spectrum of benzene," Chem. Phys. **20,** 259–269 (1977).
8. G. R. Long and S. E.Bialkowski, "Pulsed infrared laser thermal lens spectrophotometric determination of trace-level gas-phase analytes: quantitation of parts per billion dichlorodifluoromethane," Anal. Chem. **56,** 2806–2891 (1984).
9. S. E. Bialkowski and G. R. Long, "Quantitative discrimination of gas-phase species based on single-wavelength nonlinear intensity dependent pulsed infrared laser excited photothermal deflection signals," Anal. Chem. **59,** 873–879 (1987).
10. P. E. Poston and J. M. Harris, "Excited-state calorimetry studies of triplet benzophenone using time-resolved photothermal beam deflection spectroscopy," J. Am. Chem. Soc. **112,** 644–650 (1990).
11. D. J. McGraw, J. Michealson, and J. M. Harris, "Anharmonic forced Rayleigh scattering: a technique for the study of saturated absorption in liquids," J. Chem. Phys. **86,** 2536–2547 (1987).
12. X. R. Zu and J. M. Harris, "Influence of photoisomerization on saturated absorption of 3,3'-diethyloxadicarbocyanine iodide (DODCI) studied by diffraction from laser-induced anharmonic thermal gratings," Chem. Phys. **124,** 321–332 (1988).

13. X. R. Zu and J. M. Harris, "Nonlinear absorption by all-*trans*-β-carotene studied by diffraction from laser-induced anharmonic thermal gratings," J. Phys. Chem. **93,** 75–83 (1989).
14. D. M. Cox, "Pulsed optoacoustic detection of multiple photon excitation in molecules," Opt. Commun. **24,** 336–340 (1987).
15. S. L. Chin, D. K. Evans, R. D. McAlpine, and W. N. Selander, "Single-pulse photoacoustic technique for measuring IR multiphoton absorption by polyatomic molecules," Appl. Opt. **21,** 65–68 (1982).
16. T. A. Seder and E. Weitz, "Photoacoustic measurements of multiple-photon infrared absorption by alkyl chlorides and hexadienes," Chem. Phys. Lett. **104,** 545–551 (1984).
17. C. R. Giuliano and L. D. Hess, "Nonlinear absorption of light: optical saturation of electronic transitions in organic molecules with high intensity laser radiation," IEEE J. Quantum Electron. **QE-3,** 358–367 (1967).
18. J. D. Winefordner and M. Rutledge, "Comparison in calculated detection limits in molecular absorption, molecular luminescence, Raman, molecular ionization, and photothermal spectrometry," Appl. Spectrosc. **30,** 377–391 (1985).